

A Variational Phase-Field Model For Ductile Fracture with Coalescence Dissipation

USNCCM 16

Tianchen (Gary) Hu ^{1,*} John Dolbow ¹
Brandon Talamini ² Andrew Stershic ² Michael Tupek ²

¹Duke University

²Sandia National Laboratories

*Presenting

July 26th, 2021

Overview

Introduction

Theory

- Thermodynamics
- The variational statement
- Constitutive choices
- Model construction

Numerical Examples

- Three-point bending
- The Sandia Fracture Challenge
- Oxide spallation in high temperature heat exchangers

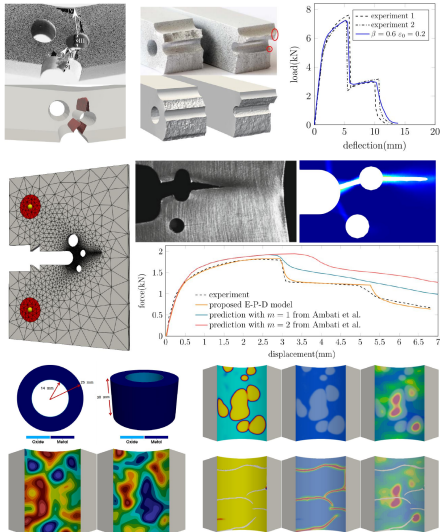
Conclusion

References

There exist many approaches to modeling plasticity in the context of phase-field fracture [1, 2, 3, 4, 5, 6, 7, 8].

We propose a variational framework for phase-field modeling of fracture in general dissipative solids [9, 10]. The framework accounts for:

- inertial effects, large deformation kinematics, and newtonian viscosity;
- inelastic deformation and associative flow rules;
- rate sensitivity of plastic deformation;
- viscous regularization of crack propagation;
- thermal effects including heat conduction, heat convection, and heat generation from dissipative mechanisms.



Introduction

Theory

Thermodynamics

The variational statement

Constitutive choices

Model construction

Numerical Examples

Three-point bending

The Sandia Fracture Challenge

Oxide spallation in high temperature heat exchangers

Conclusion

References

- Working with the Helmholtz free energy density ψ , variables we are concerned with are

$$\Phi, \quad \mathbf{F}^p, \quad \bar{\varepsilon}^p, \quad d, \quad T.$$

- Conservations and thermodynamic laws:

$$\dot{\rho}_0 = 0,$$

$$\rho_0 \mathbf{a} = \nabla \cdot \mathbf{P} + \rho_0 \mathbf{b},$$

$$\mathbf{P}\mathbf{F} = \mathbf{F}\mathbf{P}^T,$$

$$f - \nabla \cdot \boldsymbol{\xi} = 0,$$

$$\dot{u} + \dot{k} = \mathcal{P}^{\text{ext}} + \rho_0 q - \nabla \cdot \mathbf{h},$$

$$\dot{s}^{\text{int}} = \dot{s} - \frac{\rho_0 q}{T} + \nabla \cdot \frac{\mathbf{h}}{T} \geq 0.$$

- Working with the Helmholtz free energy density ψ , variables we are concerned with are

$$\Phi, \quad \mathbf{F}^p, \quad \bar{\varepsilon}^p, \quad d, \quad T.$$

- Conservations and thermodynamic laws:

$$\dot{\rho}_0 = 0,$$

$$\rho_0 \mathbf{a} = \nabla \cdot \mathbf{P} + \rho_0 \mathbf{b},$$

$$\mathbf{P}\mathbf{F} = \mathbf{F}\mathbf{P}^T,$$

$$f - \nabla \cdot \boldsymbol{\xi} = 0,$$

$$\dot{u} + \dot{k} = \mathcal{P}^{\text{ext}} + \rho_0 q - \nabla \cdot \mathbf{h},$$

$$\dot{s}^{\text{int}} = \dot{s} - \frac{\rho_0 q}{T} + \nabla \cdot \frac{\mathbf{h}}{T} \geq 0.$$

- Generalized forces are

$$\begin{aligned} \mathbf{P} &= \mathbf{P}^{\text{eq}} + \mathbf{P}^{\text{vis}}, \quad \mathbf{T} = \mathbf{T}^{\text{eq}} + \mathbf{T}^{\text{vis}}, \quad Y = Y^{\text{eq}} + Y^{\text{vis}}, \\ f &= f^{\text{eq}} + f^{\text{vis}}, \quad \boldsymbol{\xi} = \boldsymbol{\xi}^{\text{eq}} + \boldsymbol{\xi}^{\text{vis}}, \end{aligned}$$

- Following the Coleman-Noll procedure:

$$\begin{aligned} \mathbf{P}^{\text{eq}} &= \psi, \mathbf{F}, \quad \mathbf{T}^{\text{eq}} = \psi, \mathbf{F}^p, \quad Y^{\text{eq}} = \psi, \bar{\varepsilon}^p, \\ f^{\text{eq}} &= \psi, d, \quad \boldsymbol{\xi}^{\text{eq}} = \psi, \nabla d, \quad -s = \psi, T. \end{aligned}$$

- Viscous forces follow from the dual kinetic potential Δ^* :

$$\begin{aligned} \mathbf{P}^{\text{vis}} &= \Delta^*, \quad \mathbf{T}^{\text{vis}} = \Delta^*, \quad Y^{\text{vis}} = \Delta^*, \\ f^{\text{vis}} &= \Delta^*, \quad \boldsymbol{\xi}^{\text{vis}} = \Delta^*, \end{aligned}$$

- To satisfy the second law:

$$\delta = \mathbf{P}^{\text{vis}} : \dot{\mathbf{F}} + \mathbf{T}^{\text{vis}} : \dot{\mathbf{F}}^p + Y^{\text{vis}} \dot{\bar{\varepsilon}}^p + f^{\text{vis}} \dot{d} + \boldsymbol{\xi}^{\text{vis}} \cdot \nabla \dot{d} \geq 0.$$

With $\mathcal{V} = \{\dot{\phi}, \dot{\mathbf{F}}^p, \dot{\bar{\varepsilon}}^p, \dot{d}\}$:

$$\begin{aligned}(\mathcal{V}, \dot{s}, T) &= \arg \left(\inf_{\mathcal{V}, \dot{s}} \sup_T L \right), \\ L &= \int_{\Omega_0} \varphi \, dV - \mathcal{P}^{\text{ext}}, \\ \varphi &= \dot{k} + \dot{u} + \Delta^* - T\dot{s} - \chi,\end{aligned}$$

$$L = \int_{\Omega_0} \left[\dot{\psi}^e + \psi^{e*} + \dot{\psi}^p + \psi^{p*} + \dot{\psi}^f + \psi^{f*} - T\dot{s} - \chi \right] dV - \mathcal{P}^{\text{ext}},$$

subject to $\mathbf{L}(\mathbf{Z})\dot{\mathbf{Z}} = \mathbf{0}$.

Option 1 (Compressible Neo-Hookean):

$$\begin{aligned}\psi^e &= g\psi_{\langle A \rangle}^e + \psi_{\langle I \rangle}^e, \\ \psi_{\langle A \rangle}^e &= \mathbb{H}_1(J) \left\{ \frac{1}{2}K \left[\frac{1}{2}(J^2 - 1) - \ln(J) \right] \right\} \\ &\quad + \frac{1}{2}G (\bar{\mathbf{C}} : \mathbf{C}^{p-1} - 3), \\ \psi_{\langle I \rangle}^e &= (1 - \mathbb{H}_1(J)) \left\{ \frac{1}{2}K \left[\frac{1}{2}(J^2 - 1) - \ln(J) \right] \right\}.\end{aligned}$$

Option 2 (Hencky):

$$\begin{aligned}\psi^e &= g\psi_{\langle A \rangle}^e + \psi_{\langle I \rangle}^e, \\ \psi_{\langle A \rangle}^e &= \frac{1}{2}K \langle \text{tr}(\boldsymbol{\varepsilon}^e) \rangle_+^2 + G \text{dev } \boldsymbol{\varepsilon}^e : \text{dev } \boldsymbol{\varepsilon}^e, \\ \psi_{\langle I \rangle}^e &= \frac{1}{2}K \langle \text{tr}(\boldsymbol{\varepsilon}^e) \rangle_-^2, \\ \boldsymbol{\varepsilon}^e &= \frac{1}{2} \ln(\mathbf{C}^e).\end{aligned}$$

$$L = \int_{\Omega_0} \left[\dot{\psi}^e + \psi^{e*} + \dot{\psi}^p + \psi^{p*} + \dot{\psi}^f + \psi^{f*} - T\dot{s} - \chi \right] dV - \mathcal{P}^{\text{ext}},$$

subject to $\mathbf{L}(\mathbf{Z})\dot{\mathbf{Z}} = \mathbf{0}$.

Newtonian viscosity:

$$\begin{aligned}\psi^{e*} &= gJ \left[\frac{1}{2} \zeta \operatorname{tr}(\mathbf{d})^2 + \eta \mathbf{d} : \mathbf{d} \right], \\ \mathbf{d} &= \operatorname{sym} \left(\dot{\mathbf{F}} \mathbf{F}^{-1} \right).\end{aligned}$$

$$L = \int_{\Omega_0} \left[\dot{\psi}^e + \psi^{e*} + \dot{\psi}^p + \psi^{p*} + \dot{\psi}^f + \psi^{f*} - T\dot{s} - \chi \right] dV - \mathcal{P}^{\text{ext}},$$

subject to $\mathbf{L}(\mathbf{Z})\dot{\mathbf{Z}} = \mathbf{0}$.

Flow rule constraints:

$$\text{tr} \left(\dot{\mathbf{F}}^p \mathbf{F}^{p-1} \right) = 0,$$

$$\left\| \dot{\mathbf{F}}^p \mathbf{F}^{p-1} \right\|^2 - \frac{3}{2} |\dot{\bar{\varepsilon}}^p|^2 = 0.$$

Remark (Flow rule)

The joint minimization problem

$$\left(\dot{\mathbf{F}}^p, \dot{\bar{\varepsilon}}^p \right) = \arg \inf_{\dot{\mathbf{F}}^p, \dot{\bar{\varepsilon}}^p} \left[\mathbf{T}^{\text{eq}} : \dot{\mathbf{F}}^p + Y^{\text{eq}} \dot{\bar{\varepsilon}}^p + \Delta^* \right]$$

recovers the Prandtl-Reuss flow rule:

$$\dot{\mathbf{F}}^p \mathbf{F}^{p-1} = \dot{\bar{\varepsilon}}^p \mathbf{N}^p, \quad \mathbf{N}^p = \sqrt{\frac{3}{2}} \frac{\text{dev}(\mathbf{M})}{\|\text{dev}(\mathbf{M})\|},$$

and the loading/unloading conditions:

$$\phi^p \leqslant 0, \quad \dot{\bar{\varepsilon}}^p \geqslant 0, \quad \phi^p \dot{\bar{\varepsilon}}^p = 0,$$

$$\phi^p = \|\text{dev}(\mathbf{M})\| - \sqrt{\frac{2}{3}} \left(Y^{\text{eq}} + Y^{\text{vis}} \right).$$

$$L = \int_{\Omega_0} \left[\dot{\psi}^e + \psi^{e*} + \dot{\psi}^p + \psi^{p*} + \dot{\psi}^f + \psi^{f*} - T\dot{s} - \chi \right] dV - \mathcal{P}^{\text{ext}},$$

subject to $\mathbf{L}(\mathbf{Z})\dot{\mathbf{Z}} = \mathbf{0}$.

$$\psi^p = ?$$

$$\psi^{p*} = ?$$

$$L = \int_{\Omega_0} \left[\dot{\psi}^e + \psi^{e*} + \dot{\psi}^p + \psi^{p*} + \dot{\psi}^f + \psi^{f*} - T\dot{s} - \chi \right] dV - \mathcal{P}^{\text{ext}},$$

subject to $\mathbf{L}(\mathbf{Z})\dot{\mathbf{Z}} = \mathbf{0}$.

Fracture energy density:

$$\psi^f = \frac{\mathcal{G}_c}{c_0 l} (\alpha + l^2 \nabla d \cdot \nabla d).$$

Viscous regularization:

$$\psi^{f*} = ?.$$

Remark (Propagation envelope)

The fracture propagation envelope follows as:

$$\begin{aligned}\phi^f &= \nabla \cdot \frac{2\mathcal{G}_c l}{c_0} \nabla d - \left(\frac{\mathcal{G}_c}{c_0 l} \alpha_{,d} + \psi^d + f^{\text{vis}} \right), \\ \psi^d &= \psi_{,d}^e + \psi_{,d}^p.\end{aligned}$$

Irreversibility constraint:

$$\dot{d} \geq 0.$$

$$\alpha = ?$$

$$g = ?$$

$$L = \int_{\Omega_0} \left[\dot{\psi}^e + \psi^{e*} + \dot{\psi}^p + \psi^{p*} + \dot{\psi}^f + \psi^{f*} - T\dot{s} - \chi \right] dV - \mathcal{P}^{\text{ext}},$$

subject to $\mathbf{L}(\mathbf{Z})\dot{\mathbf{Z}} = \mathbf{0}$.

Fourier potential describes heat conduction:

$$\begin{aligned}\chi &= \frac{1}{2}\kappa\mathbf{g} \cdot \mathbf{g}, \\ \mathbf{g} &= -\nabla T/T.\end{aligned}$$

$$L = \int_{\Omega_0} [\dot{\psi}^e + \psi^{e*} + \dot{\psi}^p + \psi^{p*} + \dot{\psi}^f + \psi^{f*} - T\dot{s} - \chi] \, dV - \mathcal{P}^{\text{ext}},$$

subject to $\mathbf{L}(\mathbf{Z})\dot{\mathbf{Z}} = \mathbf{0}$.

The external power expenditure \mathcal{P}^{ext} is defined as

$$\begin{aligned} \mathcal{P}^{\text{ext}} = & \underbrace{\int_{\Omega_0} \rho_0 \mathbf{b} \cdot \dot{\phi} \, dV}_{\text{body force}} + \underbrace{\int_{\partial_t \Omega_0} \mathbf{t} \cdot \dot{\phi} \, dA}_{\text{surface traction}} + \underbrace{\int_{\partial_h \Omega_0} \bar{h}_n \ln\left(\frac{T}{T_0}\right) \, dA}_{\text{external heat flux}} \\ & + \underbrace{\int_{\partial_r \Omega_0} h \left[T - T_0 \ln\left(\frac{T}{T_0}\right) \right] \, dA}_{\text{external heat convection}} - \underbrace{\int_{\Omega_0} \rho_0 q \ln\left(\frac{T}{T_0}\right) \, dV}_{\text{heat source}}, \end{aligned}$$

Plasticity and fracture envelopes

$$\phi^p = \|\text{dev}(\mathbf{M})\| - \sqrt{\frac{2}{3}} (\psi_{,\bar{\varepsilon}^p}^p + \psi_{,\dot{\bar{\varepsilon}}^p}^{p*}) \leqslant 0,$$

$$\phi^f = \nabla \cdot \frac{2\mathcal{G}_c l}{c_0} \nabla d - \left(\frac{\mathcal{G}_c}{c_0 l} \alpha_{,d} + \psi_{,d}^e + \psi_{,d}^p + \psi_{,d}^{f*} \right) \leqslant 0.$$

Version 0

Resulting envelopes:

Constitutive choices:

$$\psi^p = \sigma_y \bar{\varepsilon}^p + \frac{1}{2} H \bar{\varepsilon}^{p2},$$

$$\psi^{p*} = 0,$$

$$\psi^{f*} = \frac{1}{2} v d \ddot{d},$$

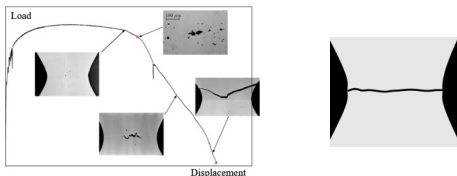
$$\alpha = d^2,$$

$$g = (1 - d)^2.$$

$$\|\text{dev}(\mathbf{M})\| - \sqrt{\frac{2}{3}} \psi_{,\bar{\varepsilon}^p}^p \leqslant 0,$$

$$\nabla \cdot \frac{2\mathcal{G}_c l}{c_0} \nabla d - \left(\frac{\mathcal{G}_c}{c_0 l} \alpha_{,d} + \psi_{,d}^e \right) \leqslant v \dot{d}.$$

Issue: Crack propagates along the plastic zone in reality.



Plasticity and fracture envelopes

$$\phi^p = \|\text{dev}(\mathbf{M})\| - \sqrt{\frac{2}{3}} (\psi_{,\bar{\varepsilon}^p}^p + \psi_{,\dot{\bar{\varepsilon}}^p}^{p*}) \leqslant 0,$$

$$\phi^f = \nabla \cdot \frac{2G_c l}{c_0} \nabla d - \left(\frac{G_c}{c_0 l} \alpha_{,d} + \psi_{,d}^e + \psi_{,d}^p + \psi_{,d}^{f*} \right) \leqslant 0.$$

Version 1

Resulting envelopes:

Constitutive choices:

$$\psi^p = \textcolor{red}{g} \left(\sigma_y \bar{\varepsilon}^p + \frac{1}{2} H \bar{\varepsilon}^{p2} \right),$$

$$\psi^{p*} = 0,$$

$$\psi^{f*} = \frac{1}{2} v d^2,$$

$$\alpha = d^2,$$

$$g = (1 - d)^2.$$

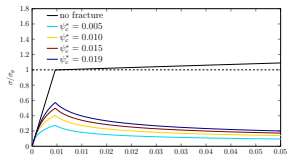
$$\|\text{dev}(\mathbf{M})\| - \sqrt{\frac{2}{3}} \psi_{,\bar{\varepsilon}^p}^p \leqslant 0,$$

$$\nabla \cdot \frac{2G_c l}{c_0} \nabla d - \left(\frac{G_c}{c_0 l} \alpha_{,d} + \psi_{,d}^e + \psi_{,d}^p \right) \leqslant v \dot{d}.$$

Improvement: Fracture and plasticity are now strongly coupled.



Issue: The response is altered by the onset of damage.



Plasticity and fracture envelopes

$$\begin{aligned}\phi^p &= \|\text{dev}(\boldsymbol{M})\| - \sqrt{\frac{2}{3}} \left(\psi_{,\bar{\varepsilon}^p}^p + \psi_{,\dot{\bar{\varepsilon}}^p}^{p*} \right) \leqslant 0, \\ \phi^f &= \boldsymbol{\nabla} \cdot \frac{2\mathcal{G}_c l}{c_0} \boldsymbol{\nabla} d - \left(\frac{\mathcal{G}_c}{c_0 l} \alpha_{,d} + \psi_{,d}^e + \psi_{,d}^p + \psi_{,d}^{f*} \right) \leqslant 0.\end{aligned}$$

Version 2

Resulting envelopes:

Constitutive choices:

$$\psi^p = g \left(\sigma_y \bar{\varepsilon}^p + \frac{1}{2} H \bar{\varepsilon}^{p2} \right),$$

$$\psi^{p*} = 0,$$

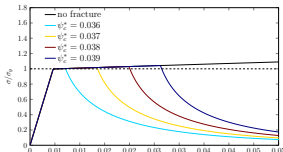
$$\psi^{f*} = \frac{1}{2} v d^2,$$

$$\alpha = \textcolor{red}{d},$$

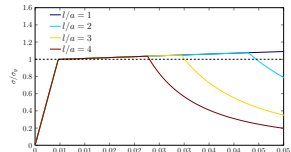
$$g = (1 - d)^2.$$

$$\begin{aligned}\|\text{dev}(\boldsymbol{M})\| - \sqrt{\frac{2}{3}} \psi_{,\bar{\varepsilon}^p}^p &\leqslant 0, \\ \boldsymbol{\nabla} \cdot \frac{2\mathcal{G}_c l}{c_0} \boldsymbol{\nabla} d - \left(\frac{\mathcal{G}_c}{c_0 l} \textcolor{red}{\alpha}_{,d} + \psi_{,d}^e + \psi_{,d}^p \right) &\leqslant v \dot{d}.\end{aligned}$$

Improvement: A purely elastoplastic stage.



Issue: The response is regularization-length dependent.



Plasticity and fracture envelopes

$$\phi^p = \|\text{dev}(\mathbf{M})\| - \sqrt{\frac{2}{3}} (\psi_{,\bar{\varepsilon}^p}^p + \psi_{,\dot{\bar{\varepsilon}}^p}^{p*}) \leqslant 0,$$

$$\phi^f = \nabla \cdot \frac{2\mathcal{G}_c l}{c_0} \nabla d - \left(\frac{\mathcal{G}_c}{c_0 l} \alpha_{,d} + \psi_{,d}^e + \psi_{,d}^p + \psi_{,d}^{f*} \right) \leqslant 0.$$

Version 3

Resulting envelopes:

Constitutive choices:

$$\psi^p = g \left(\sigma_y \bar{\varepsilon}^p + \frac{1}{2} H \bar{\varepsilon}^{p2} \right),$$

$$\psi^{p*} = 0,$$

$$\psi^{f*} = \frac{1}{2} v d^2,$$

$$\alpha = d,$$

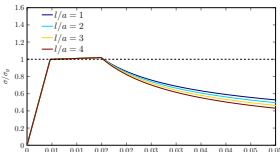
$$g = \frac{(1-d)^2}{(1-d)^2 + md(1-0.5d)}.$$

$$\|\text{dev}(\mathbf{M})\| - \sqrt{\frac{2}{3}} \psi_{,\bar{\varepsilon}^p}^p \leqslant 0,$$

$$\nabla \cdot \frac{2\mathcal{G}_c l}{c_0} \nabla d - \left(\frac{\mathcal{G}_c}{c_0 l} \alpha_{,d} + \psi_{,d}^e + \psi_{,d}^p \right) \leqslant v d.$$

Improvement: The response is regularization-length dependent.

Next: What if we incorporate thermal effects?



Plasticity and fracture envelopes

$$\begin{aligned}\phi^p &= \|\operatorname{dev}(\mathbf{M})\| - \sqrt{\frac{2}{3}} \left(\psi_{,\bar{\varepsilon}^p}^p + \psi_{,\dot{\bar{\varepsilon}}^p}^{p*} \right) \leq 0, \\ \phi^f &= \nabla \cdot \frac{2G_c l}{c_0} \nabla d - \left(\frac{G_c}{c_0 l} \alpha_{,d} + \psi_{,d}^e + \psi_{,d}^p + \psi_{,d}^{f*} \right) \leq 0.\end{aligned}$$

Version 4

Resulting envelopes:

Constitutive choices:

$$\psi^p = (1 - Q) g \sigma_y^T \bar{\varepsilon}^p, \quad \psi^{p*} = Q g \sigma_y^T \dot{\bar{\varepsilon}}^p,$$

$$\sigma_y^T = \sigma_0 \exp \left(\frac{Q}{RT} \right),$$

$$\psi^{f*} = \frac{1}{2} v d^2,$$

$$\alpha = d,$$

$$g = \frac{(1-d)^2}{(1-d)^2 + md(1-0.5d)}.$$

$$\|\operatorname{dev}(\mathbf{M})\| - \sqrt{\frac{2}{3}} \left(\psi_{,\bar{\varepsilon}^p}^p + \psi_{,\dot{\bar{\varepsilon}}^p}^{p*} \right) \leq 0,$$

$$\nabla \cdot \frac{2G_c l}{c_0} \nabla d - \left(\frac{G_c}{c_0 l} \alpha_{,d} + \psi_{,d}^e + \psi_{,d}^p \right) \leq v \dot{d}.$$

The variational framework also accounts for heat generation due to dissipative mechanisms:

$$\rho_0 c_v \dot{T} = \rho_0 q + \nabla \cdot \kappa \nabla T + \delta + \delta_T,$$

$$\delta = \mathbf{P}^{\text{vis}} : \dot{\mathbf{F}} + \psi_{,\dot{\bar{\varepsilon}}^p}^{p*} \dot{\bar{\varepsilon}}^p + \psi_{,d}^{f*} \dot{d},$$

$$\delta_T = \psi_{,\dot{\bar{\varepsilon}}^p}^{p*} \dot{\bar{\varepsilon}}^p T.$$

Issue: To get a temperature increase, we need $Q \geq \frac{Q}{Q + RT}$.

Plasticity and fracture envelopes

$$\phi^p = \|\text{dev}(\mathbf{M})\| - \sqrt{\frac{2}{3}} \left(\psi_{,\bar{\varepsilon}^p}^p + \psi_{,\dot{\bar{\varepsilon}}^p}^{p*} \right) \leq 0,$$

$$\phi^f = \nabla \cdot \frac{2\mathcal{G}_c l}{c_0} \nabla d - \left(\frac{\mathcal{G}_c}{c_0 l} \alpha_{,d} + \psi_{,d}^e + \psi_{,d}^p + \psi_{,d}^{f*} \right) \leq 0.$$

Version 5

Resulting envelopes:

Constitutive choices:

$$\psi^p = 0, \quad \psi^{p*} = g \sigma_y^T \dot{\bar{\varepsilon}}^p,$$

$$\sigma_y^T = \sigma_0 \exp \left(\frac{Q}{RT} \right),$$

$$\psi^{f*} = \frac{1}{2} v \dot{d}^2 + \frac{\mathcal{G}_c}{c_0 l} (1 - \mathbf{C}) \dot{d}$$

$$-\frac{\mathcal{G}_c}{c_0 l} (1 - \beta) \left[1 - \exp \left(-\frac{\bar{\varepsilon}^p}{\varepsilon_0} \right) \right] \dot{d},$$

$$\alpha = \mathbf{C} d.$$

$$\|\text{dev}(\mathbf{M})\| - \sqrt{\frac{2}{3}} \psi_{,\bar{\varepsilon}^p}^{p*} \leq 0,$$

$$\nabla \cdot \frac{2\mathcal{G}_c l}{c_0} \nabla d - \left(\widehat{\mathcal{G}_c} + \psi_{,d}^e + \psi_{,d}^p \right) \leq v \dot{d}.$$

The fracture toughness is “degraded” by plastic deformation:

$$\widehat{\mathcal{G}_c} = g^c \mathcal{G}_c, \quad g^c = 1 - (1 - \beta) \left[1 - \exp \left(-\frac{\bar{\varepsilon}^p}{\varepsilon_0} \right) \right].$$

To satisfy the second law, part of the fracture process is made dissipative with the constraint:

$$0 < \mathbf{C} \leq \beta.$$

Introduction

Theory

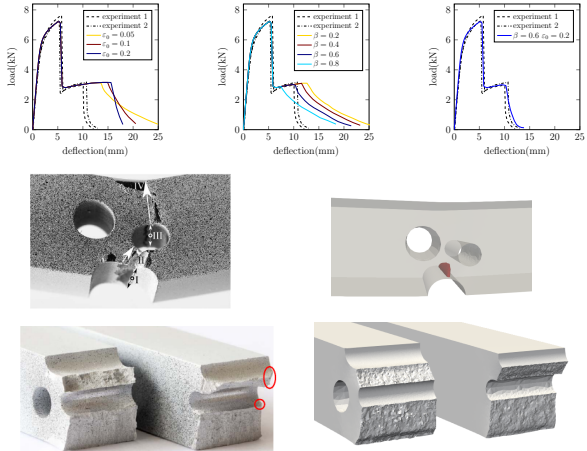
- Thermodynamics
- The variational statement
- Constitutive choices
- Model construction

Numerical Examples

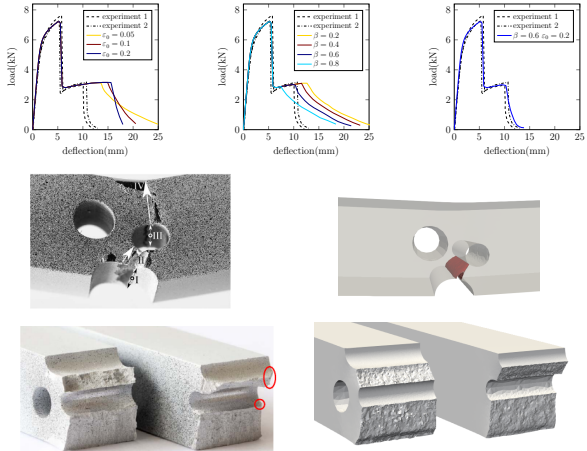
- Three-point bending
- The Sandia Fracture Challenge
- Oxide spallation in high temperature heat exchangers

Conclusion

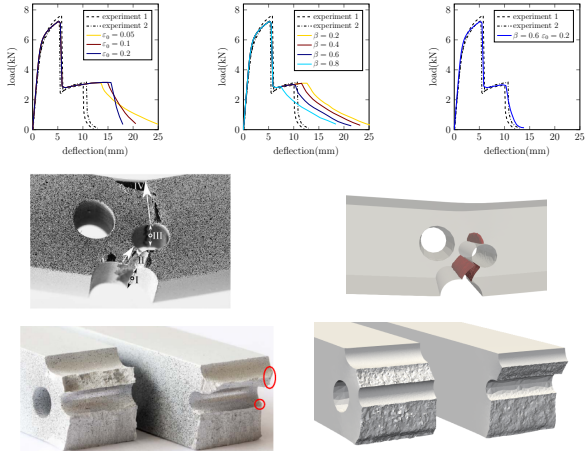
References



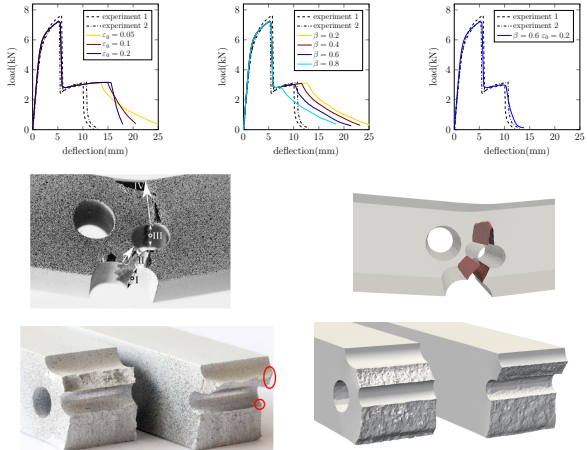
- A **three-point bending** experiment is simulated.
- The **aluminum** specimen is modeled as a **compressible Neo-Hookean** material, with **linear hardening**, $\mathcal{Q} = 1$.
- **Coalescence dissipation** is included. The effects of β and ε_0 are investigated in a 2D setting.
- Parameters are calibrated based on a **tensile tension test**.
- “Shear lips” are not captured by numerical simulations.
- Crack paths and load deflection curves have **excellent agreement** with the experiment.



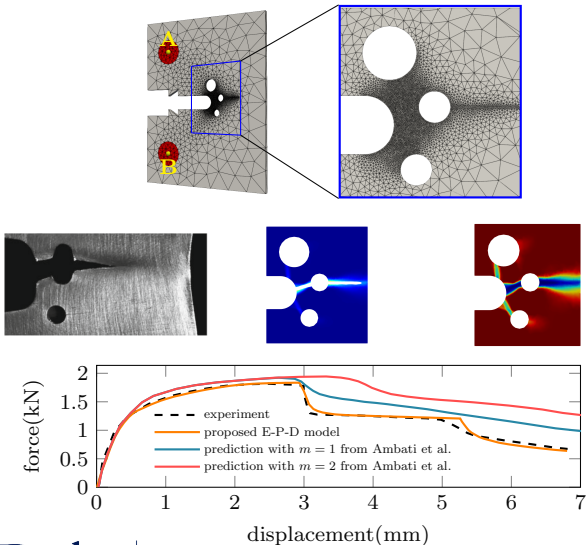
- A **three-point bending** experiment is simulated.
- The **aluminum** specimen is modeled as a **compressible Neo-Hookean** material, with **linear hardening**, $\mathcal{Q} = 1$.
- **Coalescence dissipation** is included. The effects of β and ε_0 are investigated in a 2D setting.
- Parameters are calibrated based on a **tensile tension test**.
- “Shear lips” are not captured by numerical simulations.
- Crack paths and load deflection curves have **excellent agreement** with the experiment.



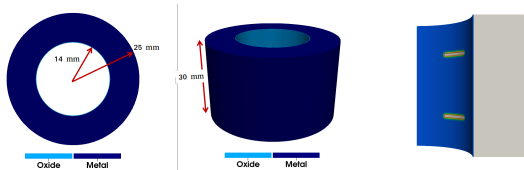
- A **three-point bending** experiment is simulated.
- The **aluminum** specimen is modeled as a **compressible Neo-Hookean** material, with **linear hardening**, $\mathcal{Q} = 1$.
- **Coalescence dissipation** is included. The effects of β and ε_0 are investigated in a 2D setting.
- Parameters are calibrated based on a **tensile tension test**.
- “Shear lips” are not captured by numerical simulations.
- Crack paths and load deflection curves have **excellent agreement** with the experiment.



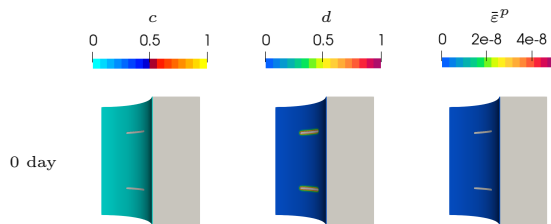
- A **three-point bending** experiment is simulated.
- The **aluminum** specimen is modeled as a **compressible Neo-Hookean** material, with **linear hardening**, $\mathcal{Q} = 1$.
- **Coalescence dissipation** is included. The effects of β and ε_0 are investigated in a 2D setting.
- Parameters are calibrated based on a **tensile tension test**.
- “Shear lips” are not captured by numerical simulations.
- Crack paths and load deflection curves have **excellent agreement** with the experiment.



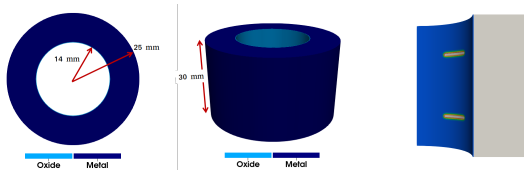
- A recent [Sandia Fracture Challenge](#).
- Material properties are calibrated using provided [tensile tension test](#) data.
- Loading pins A and B are modeled as purely elastic materials with the same constants as the specimen.
- The predicted [force-displacement curve](#) is compared with the experimental data and predictions by other existing phase-field models of ductile fracture.
- The agreement between the experiment and our simulation is [remarkable](#), both in terms of the crack path and the force-displacement curve.



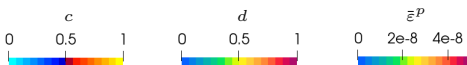
Case I: Initial transverse cracks



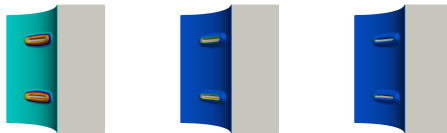
- The HTHX is simulated for 180 days under **normal operating conditions**, followed by a **shutdown** (6-hour transition).
- The HTHX is surround by **high temperature pressurized** fluids during normal operation. The temperature and the pressure of the fluids drop after shutting down.
- Most model parameters are adopted from [11].
- Creep deformation accumulates under normal operating conditions. The effective creep strain localizes around the cracks.
- Debonding occurs at weaker locations in the vicinity of the crack surfaces.
- Transverse cracks nucleate and propagate while shutting down.



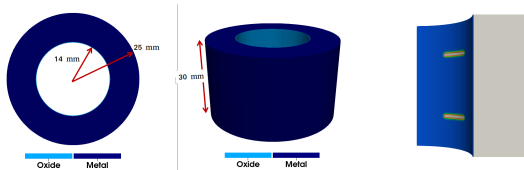
Case I: Initial transverse cracks



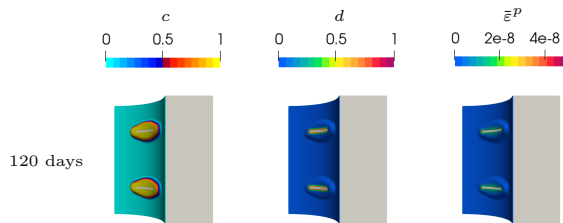
60 days



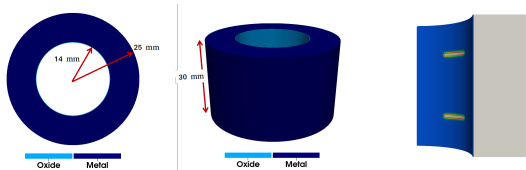
- The HTHX is simulated for 180 days under **normal operating conditions**, followed by a **shutdown** (6-hour transition).
- The HTHX is surround by **high temperature pressurized** fluids during normal operation. The temperature and the pressure of the fluids drop after shutting down.
- Most model parameters are adopted from [11].
- Creep deformation accumulates under normal operating conditions. The effective creep strain localizes around the cracks.
- Debonding occurs at weaker locations in the vicinity of the crack surfaces.
- Transverse cracks nucleate and propagate while shutting down.



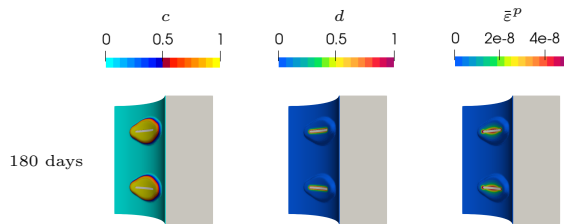
Case I: Initial transverse cracks



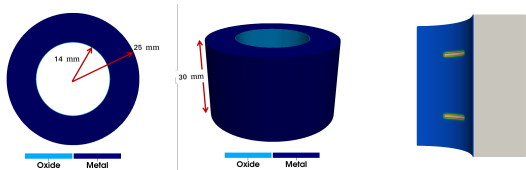
- The HTHX is simulated for 180 days under [normal operating conditions](#), followed by a [shutdown](#) (6-hour transition).
- The HTHX is surround by [high temperature pressurized](#) fluids during normal operation. The temperature and the pressure of the fluids drop after shutting down.
- Most model parameters are adopted from [11].
- Creep deformation accumulates under normal operating conditions. The effective creep strain localizes around the cracks.
- Debonding occurs at weaker locations in the vicinity of the crack surfaces.
- Transverse cracks nucleate and propagate while shutting down.



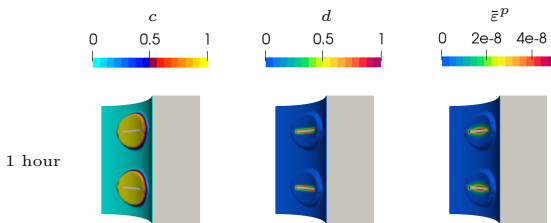
Case I: Initial transverse cracks



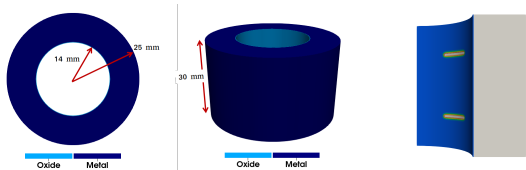
- The HTHX is simulated for 180 days under **normal operating conditions**, followed by a **shutdown** (6-hour transition).
- The HTHX is surround by **high temperature pressurized** fluids during normal operation. The temperature and the pressure of the fluids drop after shutting down.
- Most model parameters are adopted from [11].
- Creep deformation accumulates under normal operating conditions. The effective creep strain localizes around the cracks.
- Debonding occurs at weaker locations in the vicinity of the crack surfaces.
- Transverse cracks nucleate and propagate while shutting down.



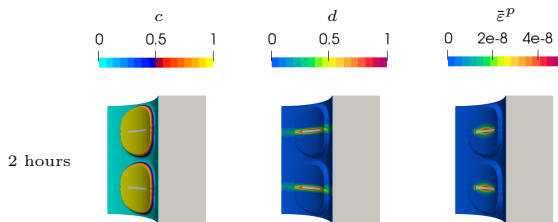
Case I: Initial transverse cracks



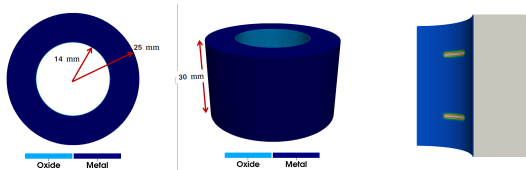
- The HTHX is simulated for 180 days under **normal operating conditions**, followed by a **shutdown** (6-hour transition).
- The HTHX is surround by **high temperature pressurized** fluids during normal operation. The temperature and the pressure of the fluids drop after shutting down.
- Most model parameters are adopted from [11].
- Creep deformation accumulates under normal operating conditions. The effective creep strain localizes around the cracks.
- Debonding occurs at weaker locations in the vicinity of the crack surfaces.
- Transverse cracks nucleate and propagate while shutting down.



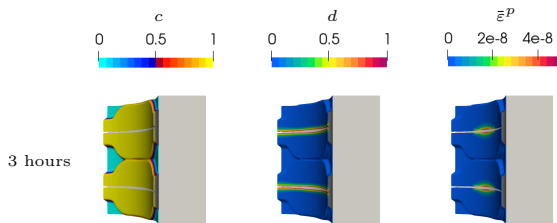
Case I: Initial transverse cracks



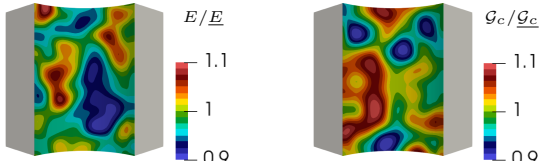
- The HTHX is simulated for 180 days under **normal operating conditions**, followed by a **shutdown** (6-hour transition).
- The HTHX is surround by **high temperature pressurized** fluids during normal operation. The temperature and the pressure of the fluids drop after shutting down.
- Most model parameters are adopted from [11].
- Creep deformation accumulates under normal operating conditions. The effective creep strain localizes around the cracks.
- Debonding occurs at weaker locations in the vicinity of the crack surfaces.
- Transverse cracks nucleate and propagate while shutting down.



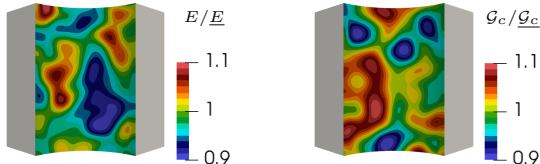
Case I: Initial transverse cracks



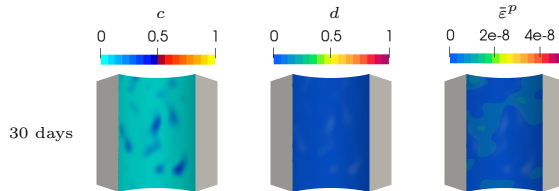
- The HTHX is simulated for 180 days under **normal operating conditions**, followed by a **shutdown** (6-hour transition).
- The HTHX is surround by **high temperature pressurized** fluids during normal operation. The temperature and the pressure of the fluids drop after shutting down.
- Most model parameters are adopted from [11].
- Creep deformation accumulates under normal operating conditions. The effective creep strain localizes around the cracks.
- Debonding occurs at weaker locations in the vicinity of the crack surfaces.
- Transverse cracks nucleate and propagate while shutting down.



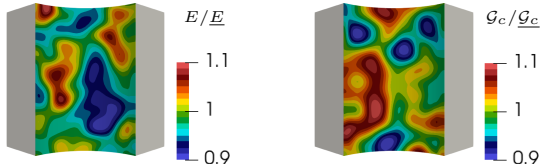
- The HTHX is simulated for 180 days under [normal operating conditions](#), followed by a [shutdown](#) (6-hour transition).
- The HTHX is surround by [high temperature pressurized](#) fluids during normal operation. The temperature and the pressure of the fluids drop after shutting down.
- Most model parameters are adopted from [11].
- Creep deformation accumulates under normal operating conditions. The effective creep strain localizes around the cracks.
- Debonding occurs at weaker locations in the vicinity of the crack surfaces.
- Transverse cracks nucleate and propagate while shutting down.



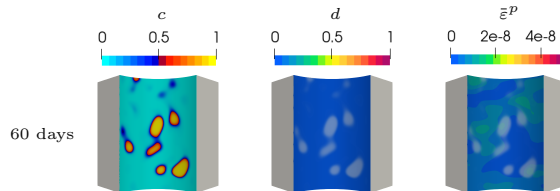
Case II: Inhomogeneous Young's modulus and Fracture toughness



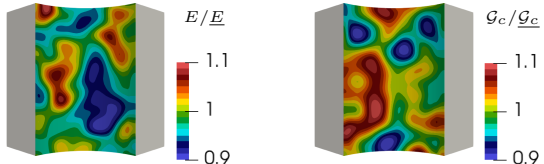
- The HTHX is simulated for 180 days under [normal operating conditions](#), followed by a [shutdown](#) (6-hour transition).
- The HTHX is surround by [high temperature pressurized](#) fluids during normal operation. The temperature and the pressure of the fluids drop after shutting down.
- Most model parameters are adopted from [11].
- Creep deformation accumulates under normal operating conditions. The effective creep strain localizes around the cracks.
- Debonding occurs at weaker locations in the vicinity of the crack surfaces.
- Transverse cracks nucleate and propagate while shutting down.



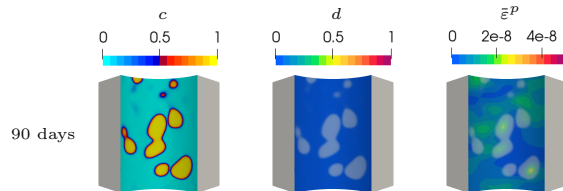
Case II: Inhomogeneous Young's modulus and Fracture toughness



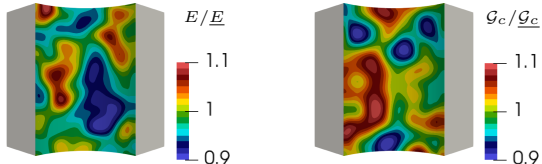
- The HTHX is simulated for 180 days under [normal operating conditions](#), followed by a [shutdown](#) (6-hour transition).
- The HTHX is surround by [high temperature pressurized](#) fluids during normal operation. The temperature and the pressure of the fluids drop after shutting down.
- Most model parameters are adopted from [11].
- Creep deformation accumulates under normal operating conditions. The effective creep strain localizes around the cracks.
- Debonding occurs at weaker locations in the vicinity of the crack surfaces.
- Transverse cracks nucleate and propagate while shutting down.



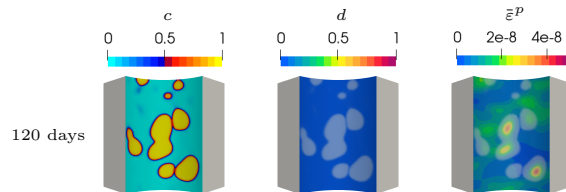
Case II: Inhomogeneous Young's modulus and Fracture toughness



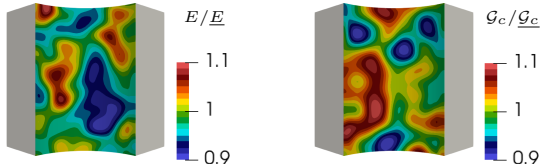
- The HTHX is simulated for 180 days under [normal operating conditions](#), followed by a [shutdown](#) (6-hour transition).
- The HTHX is surround by [high temperature pressurized](#) fluids during normal operation. The temperature and the pressure of the fluids drop after shutting down.
- Most model parameters are adopted from [11].
- Creep deformation accumulates under normal operating conditions. The effective creep strain localizes around the cracks.
- Debonding occurs at weaker locations in the vicinity of the crack surfaces.
- Transverse cracks nucleate and propagate while shutting down.



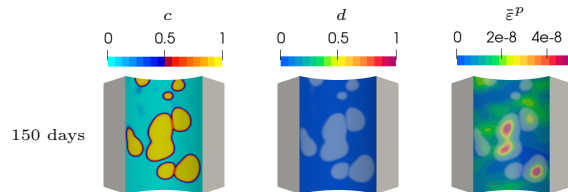
Case II: Inhomogeneous Young's modulus and Fracture toughness



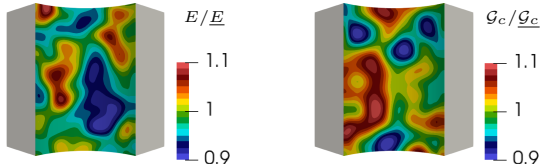
- The HTHX is simulated for 180 days under [normal operating conditions](#), followed by a [shutdown](#) (6-hour transition).
- The HTHX is surround by [high temperature pressurized](#) fluids during normal operation. The temperature and the pressure of the fluids drop after shutting down.
- Most model parameters are adopted from [11].
- Creep deformation accumulates under normal operating conditions. The effective creep strain localizes around the cracks.
- Debonding occurs at weaker locations in the vicinity of the crack surfaces.
- Transverse cracks nucleate and propagate while shutting down.



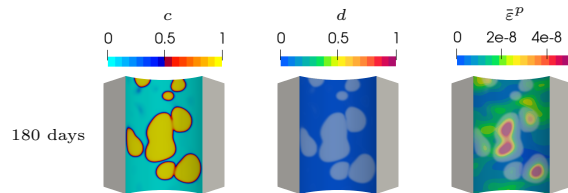
Case II: Inhomogeneous Young's modulus and Fracture toughness



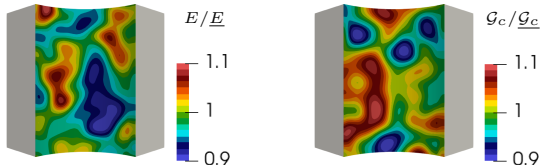
- The HTHX is simulated for 180 days under [normal operating conditions](#), followed by a [shutdown](#) (6-hour transition).
- The HTHX is surround by [high temperature pressurized](#) fluids during normal operation. The temperature and the pressure of the fluids drop after shutting down.
- Most model parameters are adopted from [11].
- Creep deformation accumulates under normal operating conditions. The effective creep strain localizes around the cracks.
- Debonding occurs at weaker locations in the vicinity of the crack surfaces.
- Transverse cracks nucleate and propagate while shutting down.



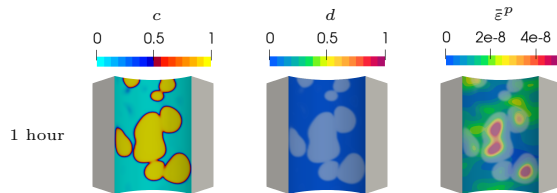
Case II: Inhomogeneous Young's modulus and Fracture toughness



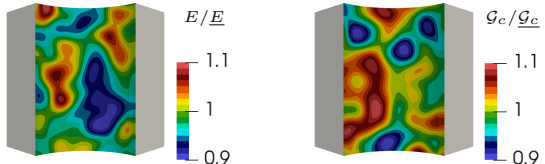
- The HTHX is simulated for 180 days under [normal operating conditions](#), followed by a [shutdown](#) (6-hour transition).
- The HTHX is surround by [high temperature pressurized](#) fluids during normal operation. The temperature and the pressure of the fluids drop after shutting down.
- Most model parameters are adopted from [11].
- Creep deformation accumulates under normal operating conditions. The effective creep strain localizes around the cracks.
- Debonding occurs at weaker locations in the vicinity of the crack surfaces.
- Transverse cracks nucleate and propagate while shutting down.



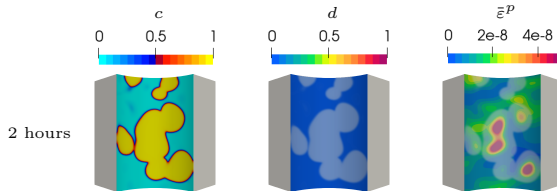
Case II: Inhomogeneous Young's modulus and Fracture toughness



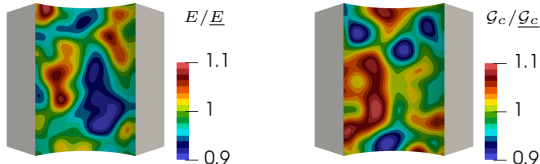
- The HTHX is simulated for 180 days under [normal operating conditions](#), followed by a [shutdown](#) (6-hour transition).
- The HTHX is surround by [high temperature pressurized](#) fluids during normal operation. The temperature and the pressure of the fluids drop after shutting down.
- Most model parameters are adopted from [11].
- Creep deformation accumulates under normal operating conditions. The effective creep strain localizes around the cracks.
- Debonding occurs at weaker locations in the vicinity of the crack surfaces.
- Transverse cracks nucleate and propagate while shutting down.



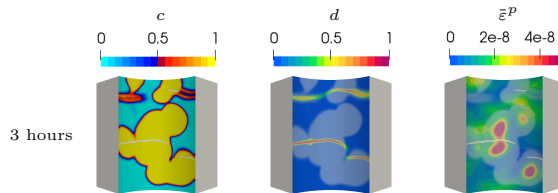
Case II: Inhomogeneous Young's modulus and Fracture toughness



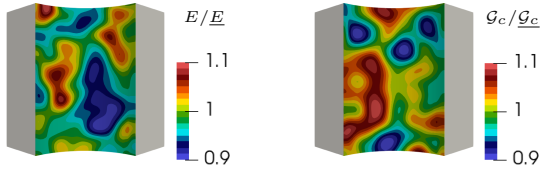
- The HTHX is simulated for 180 days under [normal operating conditions](#), followed by a [shutdown](#) (6-hour transition).
- The HTHX is surround by [high temperature pressurized](#) fluids during normal operation. The temperature and the pressure of the fluids drop after shutting down.
- Most model parameters are adopted from [11].
- Creep deformation accumulates under normal operating conditions. The effective creep strain localizes around the cracks.
- Debonding occurs at weaker locations in the vicinity of the crack surfaces.
- Transverse cracks nucleate and propagate while shutting down.



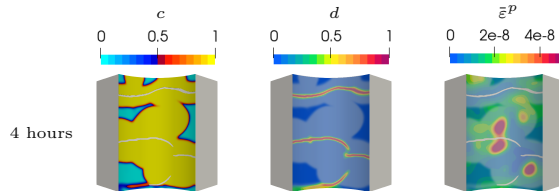
Case II: Inhomogeneous Young's modulus and Fracture toughness



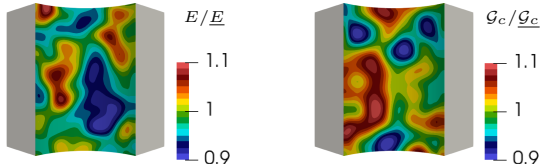
- The HTHX is simulated for 180 days under [normal operating conditions](#), followed by a [shutdown](#) (6-hour transition).
- The HTHX is surround by [high temperature pressurized](#) fluids during normal operation. The temperature and the pressure of the fluids drop after shutting down.
- Most model parameters are adopted from [11].
- Creep deformation accumulates under normal operating conditions. The effective creep strain localizes around the cracks.
- Debonding occurs at weaker locations in the vicinity of the crack surfaces.
- Transverse cracks nucleate and propagate while shutting down.



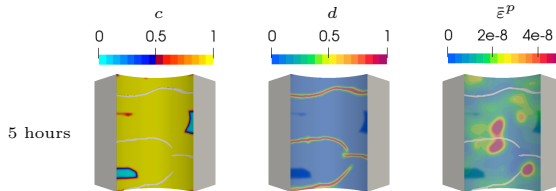
Case II: Inhomogeneous Young's modulus and Fracture toughness



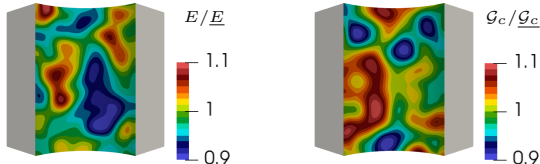
- The HTHX is simulated for 180 days under [normal operating conditions](#), followed by a [shutdown](#) (6-hour transition).
- The HTHX is surround by [high temperature pressurized](#) fluids during normal operation. The temperature and the pressure of the fluids drop after shutting down.
- Most model parameters are adopted from [11].
- Creep deformation accumulates under normal operating conditions. The effective creep strain localizes around the cracks.
- Debonding occurs at weaker locations in the vicinity of the crack surfaces.
- Transverse cracks nucleate and propagate while shutting down.



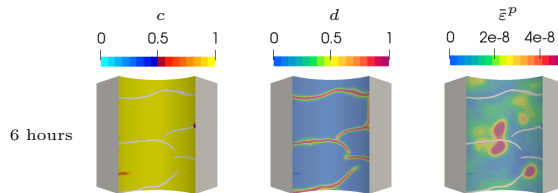
Case II: Inhomogeneous Young's modulus and Fracture toughness



- The HTHX is simulated for 180 days under [normal operating conditions](#), followed by a [shutdown](#) (6-hour transition).
- The HTHX is surround by [high temperature pressurized](#) fluids during normal operation. The temperature and the pressure of the fluids drop after shutting down.
- Most model parameters are adopted from [11].
- Creep deformation accumulates under normal operating conditions. The effective creep strain localizes around the cracks.
- Debonding occurs at weaker locations in the vicinity of the crack surfaces.
- Transverse cracks nucleate and propagate while shutting down.



Case II: Inhomogeneous Young's modulus and Fracture toughness



- The HTHX is simulated for 180 days under [normal operating conditions](#), followed by a [shutdown](#) (6-hour transition).
- The HTHX is surround by [high temperature pressurized](#) fluids during normal operation. The temperature and the pressure of the fluids drop after shutting down.
- Most model parameters are adopted from [11].
- Creep deformation accumulates under normal operating conditions. The effective creep strain localizes around the cracks.
- Debonding occurs at weaker locations in the vicinity of the crack surfaces.
- Transverse cracks nucleate and propagate while shutting down.

Concluding remarks:

- We presented a variational framework for phase-field modeling of fracture in general dissipative solids.
- Careful constitutive choices result in favorable responses:
 - unperturbed elastoplastic response;
 - regularization-length independent critical fracture strength;
 - regularization-length independent crack resistance curve.
- We introduced a novel coalescence dissipation as an alternative way of coupling fracture and plasticity.
- The model starts to look really predictive in several challenging problems.
- The flexibility of the framework is demonstrated by modeling oxide spallation in HTHXs.

Advertisements:

- All numerical results are obtained using RACCOON (a MOOSE-based application). It is open-source and massively parallel. All models are plug-n-play.
- Poster session at 5:45 - 7:00 pm, July 28th. Title: “A Variational Framework for Phase-Field Modeling of Fracture in General Dissipative Solids”.

Acknowledgements:



70 YEARS OF SCIENCE & INNOVATION

- [1] Roberto Alessi, Jean-Jacques Marigo, and Stefano Vidoli.
Gradient damage models coupled with plasticity and nucleation of cohesive cracks.
Archive for Rational Mechanics and Analysis, 214(2):575–615, November 2014.
- [2] Roberto Alessi, Jean-Jacques Marigo, and Stefano Vidoli.
Gradient damage models coupled with plasticity: Variational formulation and main properties.
Mechanics of Materials, pages 351–367, 2015.
- [3] Roberto Alessi, Jean-Jacques Marigo, Corrado Maurini, and Stefano Vidoli.
Coupling damage and plasticity for a phase-field regularisation of brittle, cohesive and ductile fracture: One-dimensional examples.
International Journal of Mechanical Sciences, 149:559–576, December 2018.
- [4] M. Ambati, T. Gerasimov, and L. De Lorenzis.
Phase-field modeling of ductile fracture.
Computational Mechanics, 55(5):1017–1040, May 2015.

- [5] Marreddy Ambati, Roland Kruse, and Laura De Lorenzis.
A phase-field model for ductile fracture at finite strains and its experimental verification.
Computational Mechanics, 57(1):149–167, 2016.
- [6] Christian Miehe, Fadi Aldakheel, and Arun Raina.
Phase field modeling of ductile fracture at finite strains: A variational gradient-extended plasticity-damage theory.
International Journal of Plasticity, 84:1–32, September 2016.
- [7] Michael J Borden, Thomas JR Hughes, Chad M Landis, Amin Anvari, and Isaac J Lee.
A phase-field formulation for fracture in ductile materials: Finite deformation balance law derivation, plastic degradation, and stress triaxiality effects.
Computer Methods in Applied Mechanics and Engineering, 312:130–166, 2016.
- [8] Michael J. Borden, Thomas J. R. Hughes, Chad M. Landis, Amin Anvari, and Isaac J. Lee.
Phase-field formulation for ductile fracture.
In Advances in Computational Plasticity: A Book in Honour of D. Roger J. Owen, volume 46, page 443. Springer International Publishing, September 2017.

- [9] Tianchen Hu, Brandon Talamini, Andrew J Stershic, Michael R Tupek, and John E Dolbow. A variational phase-field model for ductile fracture with coalescence dissipation. *Computational Mechanics*, pages 1–25, 2021.
- [10] Brandon Talamini, Michael R Tupek, Andrew J Stershic, Tianchen Hu, James W Foulk III, Jakob T Ostien, and John E Dolbow. Attaining regularization length insensitivity in phase-field models of ductile failure. *Computer Methods in Applied Mechanics and Engineering*, 384:113936, 2021.
- [11] Fei Xue, Tian-Le Cheng, and You-Hai Wen. Stress analysis of the steam-side oxide of boiler tubes: Contributions from thermal strain, interface roughness, creep, and oxide growth. *Oxidation of Metals*, 93(5):515–543, 2020.